Influence of expanding and contracting magnetic field configurations on detached plasma formation in a linear plasma device

Influence of expanding and contracting magnetic field configurations on detached plasma formation in a linear plasma device

Y. Hayashi[1*], N. Ohno[1], S. Kajita[2], H. Tanaka[1]

[1]*Graduate School of Engineering, Nagoya University, Nagoya, Aichi 464-8603, Japan*

[2]*Institute of Materials and Systems for Sustainability, Nagoya University, Nagoya, Aichi 464-8603, Japan*

(Dated:)

Abstract

We investigated the effects of magnetic field structure on detached plasma formation by simulating magnetically expanding and contracting plasma in a linear plasma device. The present study helps characterize the geometries of a conventional poloidal divertor and advanced divertors, e.g., super-X divertor. The total ion particle flux measured with a large-diameter target plate dramatically changed under the detached plasma condition compared to that in attached plasma. Under the detached plasma condition, the magnetically expanding plasma clearly exhibited a significant influence on the degradation of detached plasma formation. Further, the magnetically contracting plasma slightly enhanced the electron-ion recombination (EIR) processes. By changing the magnetic field structure from contraction to expansion, the electron density (n_e) decreased and the electron temperature (T_e) increased upstream from the recombination front, leading to the degradation of the EIR processes. The effect of the decrease in parallel flow velocity under the magnetically contracting plasma on the plasma detachment was not observed because the driven flow due to pressure gradient compensated the effect.

Corresponding author E-mail: hayashi-yuki13@ees.nagoya-u.ac.jp

I. INTRODUCTION

For divertor plate protection in future fusion devices, such as ITER and DEMO, it is necessary to reduce the electron temperature (T_e) in the scrape-off layer (SOL) due to radiation enhancement achieved by seeding impurities [1, 2]. Large heat and particle fluxes interact with these impurities and recycling particles during their transport towards the divertor. Finally, the operation with the large radiation and the momentum losses leads to a detached divertor. A volumetric recombination in the detached plasma plays an important role in the strong decrease of the ion particle flux to the divertor plate [3–5]. Under the detached plasma condition, understanding of T_e and the electron density (n_e) is crucial because the rate coefficient of electron-ion recombination (EIR), which includes radiative and three-body recombination processes, has a strong dependence on n_e and especially on T_e [6, 7]. In a simple one-dimensional model, n_e and T_e are considered by assuming the magnetic field strength to be constant during the transport towards the divertor. However, the magnetic field strength two-dimensionally varies in the divertor region.

A conventional poloidal divertor configuration accompanies the contraction of magnetic flux towards a divertor plate from the X-point. It results in the concentration of peak heat and particle fluxes at the materials, leading to serious erosion and melting. Moreover, under the detached divertor condition, the impurity radiation region moves towards the X-point as detachment proceeds to form X-point MARFE [8–10]. This condensation instability degrades the core plasma confinement and enhances the neutral pressure in main chamber. Further, the theoretical analysis suggested that impurity radiation and ionization-recombination fronts shift towards the X-point [11].

On the other hand, advanced divertors such as the X-divertor (XD) [12], super-X

divertor (SXD) [13], and snowflake divertor (SFD) [14] were proposed for handling large amount of power exhausted from the SOL and for divertor plate protection. Compared to the conventional divertor, the SFD geometry results in high poloidal flux expansion and a large plasma wetted area [14]. The magnetically expanding plasma leads to a strong reduction in peak heat that is loaded onto the divertor plate. While the SXD also accompanies poloidal flux expansion, the main role of the SXD is to reduce T_e along the magnetic field lines via long connection length in the major radius direction [15]. These advanced divertors are thought to have an advantage in stabilizing the radiation front far from the X-point, because the plasma-neutral interaction area increases towards the divertor plate through the magnetic flux expansion [16]. On the other hand, properties such as high n_e and low parallel flow velocity are preferred to produce the detached plasma effectively, because these properties enhance the volumetric recombination. The magnetically expanding plasma may be a disadvantage for the formation of detached plasma because magnetic flux expansion reduces n_e and increase the parallel flow velocity due to a contrary effect of a magnetic mirror, leading to degradation of the EIR processes.

It is necessary to investigate the effects of magnetic flux expansion and contraction on detached plasma formation. Although, in the fusion devices, it is difficult to only control the magnetic field structure in the divertor region, linear plasma devices make it possible to control the magnetic field in the upstream and downstream sides separately. In a linear plasma device NAGDIS-II, influence of magnetic flux expansion and contraction on detached plasma can be observed over the ~ 2 m long plasma. The primitive experiment in NAGDIS-II showed the degradation of detached plasma formation under the magnetically expanding plasma condition [17]. However, measurements of T_e and n_e, which determine the rate coefficient of

EIR processes, were not done. Further, the flow velocity along the magnetic field lines would be also important because the high flow velocity reduces the time required for the volumetric recombination in the limited connection length. In this study, we clarified influences of the magnetically expanding and contracting effects on the detached plasma formation with detailed parameter measurements along and across the magnetic field lines in NAGDIS-II.

In the following section, experimental setup, including the magnetic field structure in NAGDIS-II and multipoint measurement of electrostatic probes along and across the magnetic field, is described. In Sec. III, in order to investigate the effects of magnetic field structure on the plasma when the EIR processes are not dominant, the results in attached plasma are presented. After that, the results in detached plasma are described. Contribution of the present study on the fusion devices and a future work are explained in Sec. IV. Finally, we conclude in Sec. V.

II. EXPERIMENTAL SETUP

NAGDIS-II [18] generated helium plasma by a DC arc discharge in a steady state. Fig. 1 shows the magnetic field strength profiles at the center of the vacuum vessel induced by 20 solenoidal magnetic coils. In order to achieve magnetic flux expansion and contraction in the axial direction, 12 magnetic coils in upstream and 8 coils in downstream were separately operated. In the present study, the magnetic field strengths were 0.15 T in the upstream (B_u) and 0.05–0.2 T in the downstream (B_d). In order to investigate the degradation of detachment under the magnetically expanding plasma condition in detail, B_u was set to 0.15 T.

The length of the plasma column was 2.05 m from the anode, and it was terminated with a 0.12 m diameter water-cooled molybdenum target plate. We used two discharge

conditions: attached and detached plasma conditions. In former and latter cases, the discharge currents were set to 10 and 50 A, respectively. The discharge current of 10 A for attached plasma was adopted in order to reduce the heat load to an after-mentioned Mach probe. Under the attached plasma condition, the neutral pressure measured at middle position in the axis was approximately 0.4 Pa. When the additional helium gas was injected from the second gas puffing port near the target plate, the neutral pressure increased and the detached plasma was obtained. In the detached plasma condition, the neutral pressure in the vacuum vessel was fixed at approximately 2.9 Pa. In this case, both ionizing and recombining plasmas coexisted along the magnetic field. The ionizing plasma and the recombining plasma were located in upstream and downstream sides, respectively. At the recombination front, which was located between the ionizing and recombining plasmas, strong line emissions due to the volumetric recombination processes were observed.

The current to the target plate (I_{target}) was measured by applying a bias voltage of –100 V and –200 V to the target plate in the attached and detached plasmas, respectively. These bias voltages are sufficient lower than the floating potential. The diameter of the target plate is much larger than that of plasma column. Therefore, this measurement evaluated the total ion particle flux into the target plate. In addition, optical emission spectroscopy (OES) was performed from several observation windows along the magnetic field. The line of sight of an optical fiber was aligned to pass through the center of plasma column. Fast scanning electrostatic probes were also used to measure the radial profiles of n_{e} and T_{e} at upstream (up: z = 0.25 m), midstream (mid: z = 1.06 m), and downstream (end: z = 1.72 m). Here, axial position (z) was defined as the distance from the anode surface (z = 0 m). In the past experiments in NAGDIS-II [19, 20] and MAP-II [21], the anomalous probe measurements

resulted in an overestimation of T_e in the recombining plasma. It was concluded that the plasma potential fluctuation and the variation in its resistivity cause the single probe characteristics to give higher values of T_e [20]. Therefore, it was suggested to use a double probe for estimating T_e in the detached recombining plasma, because it can reduce undesirable influences from the potential fluctuation and plasma resistance due to the presence of local probe tips in the plasma and short current path between the electrodes. The validity of T_e measurements obtained by using the double probe was confirmed by comparing them with those obtained from the Thomson scattering measurement in NAGDIS-II [22], and its detail will be reported in other paper. In the present experiments, both n_e and T_e were measured by using a single probe at up-probe and a double probe at the mid and end-probe locations.

The flow velocity was also measured at z = 1.39 m by using the Mach probe illustrated in Fig. 2. Two tungsten electrodes were placed 0.5 mm inside an alumina tube. The dimension of the exposed area of each electrode was 1.0 mm in diameter. The Mach probe electrodes were aligned along the magnetic field to measure the plasma flow in the axial direction, and its position was fixed during the data acquisition. The bias voltage of the two tungsten electrodes was set to –200 V to measure the ion saturation current (I_{sat}) from upstream and downstream sides. The Mach number M_i is evaluated by the following relation [23, 24],

$$M_i = M_c \ln(I_{up} / I_{down}), \quad (1)$$

where I_{up} and I_{down} are the measured I_{sat} of the upstream and downstream electrodes, respectively. When I_{up} is greater than I_{down}, the flow direction is towards the target plate, and the sign of M_i is denoted by a plus. M_c is an important constant for the absolute determination of the flow velocity [25]. Further, M_c is determined by the calibration factor (K), which

depends on the magnetic field strength, the ratio of ion temperature (T_i) to T_e, and the collision parameters. The appropriate values of K have been discussed for the plasma under the high neutral pressure (0.3–4.7 Pa) conditions in NAGDIS-II [26]. It was concluded that inclusion of collisional effects is necessary to estimate Mach number in collisional flowing plasmas. In this study, K of 1.1 and 1.5 were used for measuring the flow velocity in attached and detached plasma cases, respectively. However, we mainly discussed the relative values of the Mach number, which is evaluated by $\ln(I_{up} / I_{down})$.

III. RESULTS AND DISCUSSION

A. Attached plasma case

1. Effects of magnetic field structure under the attached plasma condition

In this section, the effects of magnetic field structure on the attached plasma were presented, in order to compare with the case of detached plasma. The low-density plasma and low neutral pressure do not lead to plasma detachment. At the upstream region, the measured T_e was ~ 5 eV and did not depend on B_d. Figs. 3(a) and 3(b) show I_{target} and the flow velocity at z = 1.39 m as the function of B_d, respectively. Because B_u was fixed at 0.15 T, B_d = 0.15 T means straight, B_d < 0.15 T means expanding, and B_d > 0.15 T means contracting magnetic field structures in the axial direction. Fig. 3(a) shows that I_{target} slightly decreased with increasing B_d, implying a reduction of ion particle flux. Approximately 40% of I_{target} dissipated when B_d was changed from 0.05 to 0.2 T. The reduction could not be simply explained by the enhancement of the EIR processes, because T_e was more than 1 eV at the plasma center. As shown in Fig. 3(b), the flow velocity decreased when B_d > 0.15 T. These results indicated that the mirror effect decreased the flow velocity in the magnetically

contracting plasmas.

2. Particle flux reduction due to diffusion process

Here, we discuss the mechanisms of the 40% reduction of I_{target} by changing the magnetic field structure from expansion to contraction. One of the reasons for reducing I_{target} should be the decrease in the flow velocity due to the magnetic mirror effect. Second possible reason is the recombination caused by the cross-field diffusion process. Fig. 4(a) and 4(b) show the pictures of plasmas with the spatial positions at B_d of ~0.05 T and 0.2 T. When B_d ~ 0.05 T, the plasma profile was broadened owing to the magnetic flux expansion. When B_d ~ 0.2 T, on the other hand, the plasma consisted of an ionizing core (r < 10 mm) surrounded by a recombining edge (r > 10 mm) plasma, which could reduce the I_{target}. Figs. 4(c) and 4(d) show the radial profiles of n_e and T_e measured at the end-probe location. In the recombining edge (r ~ 20 mm), the cold T_e at a B_d of 0.2 T was approximately 0.4 eV, which was sufficiently low for the recombination, while T_e at a B_d of 0.05 T was higher than 1 eV. The recombining edge plasma seen in Fig. 4(b) could be explained as the radial transport from the plasma column to the edge region, followed by cooling and recombination. As shown in Fig. 4(c), n_e in magnetically contracting and expanding plasmas have different gradients. When B_d ~ 0.2 T, the profile showed a peak and the steep gradient, which could enhance the diffusion process in a cross-field direction. Under the attached plasma condition, the reduction of I_{target} was caused by the decrease in the flow velocity due to the magnetic mirror effect and the radial transport, leading to cooling and recombination in the peripheral region.

B. Detached plasma case

1. Dependence of plasma detachment on magnetic field structure

In this section, we show the results under the detached plasma condition. Figs. 5(a) and 5(b) show the I_{target} and floating potential at the target plate (ϕ_{target}) as a function of B_d. When $B_d \sim 0.15$ T and when $B_d > 0.15$ T, I_{target} was the lowest and exhibited a weak dependence on B_d. However, when $B_d < 0.15$ T, I_{target} increased as B_d decreased. The results indicated that the magnetically expanding plasma degraded the detached plasma formation. Further, as shown in Fig. 5 (b), ϕ_{target} negatively increased with decreasing B_d, indicating an increase in T_e. These results also indicated the degradation of plasma detachment due to the magnetic field expansion, because lower T_e is required to enhance the EIR processes more effectively. The reasons for the degradation of detached plasma formation could be the decrease in n_e, leading to weakening of the EIR processes. Moreover, a decrease in n_e also leads to an increase in T_e, because ion-electron coulomb coupling is the important process to reduce T_e in detached plasma. Further, it is interesting to note that the formation of plasma detachment was affected only by the magnetic field structure. Without changing the neutral pressure, the total particle flux into the target plate dramatically changed in the present condition. Under the attached plasma condition, the reduction ratio was ~ 40 % when B_d was changed from 0.05 to 0.2 T. However, under the detached plasma condition, more than 90% of I_{target} dissipated.

2. Observation of volumetric recombination

For proving the EIR, i.e., volumetric recombination processes, which depend on the magnetic field structure, OES was performed at nine ports aligned along the magnetic field line. Fig. 6 shows the axial profiles of He-I line emission intensity corresponding to the transition from highly excited level (370.5 nm: 2^3P-7^3D). Under the detached plasma

condition, the population of high-n states was likely to be determined by the EIR processes, where n is the principal quantum number. Therefore, in recombining plasma, the transitions from highly excited levels were the indications of EIR [27]. As shown in Fig. 6, the EIR processes were enhanced with increasing B_d. The peak of the bright position at z = 1.225 m was the recombination front, at which the intensity especially depended on B_d. The shift of recombination front in the axial direction was not clearly observed while B_d changed. In other words, the position of recombination front could not change more than 0.165 m, which is the distance between observation windows. As described in Sec. I, the radiation front is supposed to stabilize at different positions depending on the magnetic field configurations. This behavior was not clearly indicated from the observation of recombination front under the present condition. For investigating the position of recombination front in detail, the numerical simulation, which includes the axial profiles of n_e and T_e and particle transport, and measurements of axial profiles of these parameters are necessary, because EIR processes strongly depend on n_e and T_e.

The measurement positions of electrostatic probes are depicted in Fig. 6. Both mid-probe and end-probe were reciprocated in the plasma column where the recombination was dominant. The mid-probe and end-probe measured upstream and downstream sides from the recombination front, respectively. The changes in density upstream side from the recombination front due to controlling magnetic field structure affected the EIR processes. The influence of n_e on EIR processes is explained in next section. In the present experiment, it should be noted that the degradation of EIR processes in the magnetically expanding plasma was larger than enhancement of that in the magnetically contracting plasma.

3. Effects of electron density and temperature on recombination processes

In order to investigate the effects of n_e and T_e on the formation of plasma detachment, fast scanning electrostatic probe measurements were performed. Fig. 7 shows the radial profiles of n_e and T_e measured at upstream, midstream, and downstream locations, when B_d was changed from 0.05 to 0.2 T. At the up-probe location (Fig. 7(a) and 7(b)), the measured values of n_e and T_e were ~ 4–5 × 10^{19} m^{-3} and ~ 2–3 eV, respectively, and there was no clear dependence on B_d. Therefore, the plasma parameters in the upstream region were not affected by changing B_d, and it was possible only to control the plasma in midstream and downstream regions.

At the mid-probe location (Fig. 7(c)), the maximum value of n_e was larger when B_d ~ 0.2 T than that when B_d ~ 0.05 T. The increased density at the mid-probe location was caused by the magnetic field contraction, and it could contribute to the reduction of particle flux through the EIR processes. A strong reduction of particle flux should occur at the recombination front, which was located at downstream side from the mid-probe location. Fig. 7(d) shows the T_e, measured at mid-probe location, affected by changing the magnetic field structure. An increase in T_e was observed with a decrease in the B_d. These results support the consideration that the decrease of n_e leads to an increase in the T_e due to degradation in the coulomb coupling between electrons and ions. A high T_e could reduce the EIR processes at the recombination front under the magnetically expanding plasma condition.

At the end-probe location (Fig. 7(e)), n_e strongly reduced excepting the case where B_d ~ 0.05 T. These results were consistent with those of the particle flux measurements at the target plate. Fig. 7(f) shows the radial profiles of T_e measured at the end-probe location. When B_d ~ 0.05 T, T_e was higher than that when B_d ~ 0.2 T. This tendency was still similar to that of the

results at the mid-probe location, although the profiles were totally decreased owing to the transport through the recombination front. Because the distance between end-probe location and the target plate was only 0.33 m, the higher T_e caused lower ϕ_{target} at the $B_u > B_d$ condition.

4. Contribution of flow velocity to recombination processes

As mentioned above, the degradation of plasma detachment due to the magnetic field expansion could be caused by the decrease of n_e and the increase of T_e, leading to weakening of the EIR processes. The results of OES suggested that the magnetic field contraction slightly enhanced the EIR processes. The reduction of ion parallel flow velocity due to the mirror effect in magnetically contracting plasma could increase the coupling time between the ions and electrons, leading to a decrease of T_e and the enhancement of EIR processes. In this section, the effects of the flow velocity on the formation of plasma detachment are discussed.

Fig. 8 shows the flow velocity measured by the Mach probe at z = 1.39 m as a function of B_d. When $B_d < 0.15$ T, the flow velocity increased with increasing B_d. Further, the flow velocity did not change, when $B_d > 0.15$ T. These results contradicted the prediction that the flow velocity could be reduced due to the magnetic mirror effect by magnetic contraction. The enhancement of axial flow with increasing B_d could be caused by the plasma pressure gradient in the axial direction. As the detachment proceeds, the steep gradients in T_e and n_e could drive the flow [28]. When $B_d > 0.15$ T, the effect of magnetic mirror may also contribute to the reduction of ion flux, because the flow velocity decreased when $B_u < B_d$ under the attached plasma condition. However, under the detached plasma condition, the flow reduction due to magnetic mirror effect was not observed. The driven flow by the pressure gradient was larger

than the flow affected by the magnetic mirror effect when $B_d < 0.15$ T, and they were almost equivalent when $B_d > 0.15$ T. It was also found that EIR processes were enhanced with the increase in B_d due to the variation in T_e and n_e in the magnetically expanding plasma even though the flow velocity increased, leading to the reduction in the coupling time between the ions and electrons.

IV. CONTRIBUTION OF PRESENT STUDY TO FUSION DEVICES

In the present study, a conventional poloidal divertor configuration, which accompanies the contraction of magnetic flux towards a divertor plate, was simply simulated in the NAGDIS-II device. The magnetically contracting plasma enhanced the EIR processes in the steady state detached plasma in NAGDIS-II. Although the enhanced density is an advantage for the formation of plasma detachment, the concentration of peak heat and particle fluxes at the materials is serious problem in attached divertor regime. Because the ELMy H-mode is the required operational candidate for stationary confinement in ITER, the detached plasma at the front of the divertor interacts with the non-stationary heat loads. The transition to re-attached divertor due to re-ionization process after ELMs causes the loading of the concentrated heat onto the divertor plate in magnetically contracting plasma.

In addition, the present study simulated a magnetically expanding plasma, which is adopted in advanced divertor configurations, such as SXD and SFD. Although the magnetic expansion was found to degrade the detached plasma formation, the actual magnetic configuration in the divertor region is more complicated than the geometry in the present study. It has been reported in Ref. [29] that the SXD for MAST Upgrade accompanies both magnetic field contraction and expansion. In the SXD geometry, once the magnetic flux is

contracting from the X-point towards the divertor plate, and then it is extended in the major radius direction, accompanying the magnetic flux expansion. The magnetic field expansion has a disadvantage for reducing T_e, while it leads to a strong reduction in peak heat flux due to the increased wetted area. When the high-density region, such as an ionization front, is located in the magnetically contracting plasma, a sufficient reduction in T_e could be obtained. It can be stated that the magnetic field contraction enhances n_e and decreases T_e and following region handles the remaining plasma by magnetic field expansion. Thus, it is of interests to simulate the combination geometry of magnetic expansion and contraction. Fig. 9 shows the calculated magnetic field at the center of vacuum vessel for producing the axially localized contracting and expanding magnetic fields in NAGDIS-II. The coil current for both the magnetic coils at $z \sim 0.98$ m and 1.14 m were separately controlled, and the coil current for other coils was set to according to a magnetic field of 0.1 T. The localized magnetic expansion produces the magnetic mirror geometry with a mirror ratio of 2. The localized magnetic field contraction achieves the experiments for the geometries such as SXD.

V. CONCLUSION

In order to understand the influence of magnetic field structure on the detached plasma formation, magnetically expanding and contracting plasmas to the target plate were simulated in a linear plasma device NAGDIS-II. At first, ion flux into the attached target was measured, in order to clarify the magnetic field structure effect without the plasma detachment. Under the attached plasma condition, where the T_e was greater than 1 eV and the EIR processes were not dominant, the flow reduction due to magnetic mirror effect and cold recombining edge plasma reduced the ion flux to the target plate under the magnetically contracting plasma.

Under the detached plasma condition, larger amount (~90%) of ion flux dissipated while it was ~40% in the attached plasma by changing the magnetic field structure from expansion to contraction. Further, the enhancement mechanism of the EIR processes under the magnetically contracting plasma, as reported in Ref. [17], was investigated by using electrostatic probes for n_e, T_e, and flow measurements. The magnetically expanding plasma clearly showed the degradation of the EIR processes, and the enhancement of the EIR in magnetically contracting plasma was smaller. By changing the magnetic field structure from contraction to expansion, n_e decreased and T_e increased at the upstream side from the recombination front, leading to the degradation of EIR processes. The axial flow was driven by the steep gradient of the plasma pressure. The driven flow was larger than the flow variation due to the magnetic mirror effect under the magnetically expanding plasma and they were almost equivalent under the magnetically contracting plasma. The enhancement of EIR processes was mainly attributed to an increase in n_e and a decrease in T_e while the contribution of flow reduction due to the mirror effect was not observed.

ACKNOWLEDGEMENTS

This work was supported by JSPS KAKENHI (16H02440 and 16H06139), NIFS/NINS under the project of Formation of International Network for Scientific Collaborations, and NIFS Collaboration Research Program (NIFS17KUGM130).

References

[1] A. Kallenbach, M. Bernert, R. Dux, L. Casali, T. Eich, L. Giannone, A. Herrmann, R. McDermott, A. Mlynek, H W Müller, F. Reimold, J. Schweinzer, M. Sertoli, G. Tardini, W. Treutterer, E. Viezzer, R. Wenninger, M. Wischmeier, and the ASDEX Upgrade Team, Plasma Phys. Control. Fusion **55**, 124041 (2013).

[2] F. Reimold, M. Wischmeier, M. Bernert, S. Potzel, A. Kallenbach, H.W. Muüller, B. Sieglin, U. Stroth, and the ASDEX Upgrade Team, Nucl. Fusion **55**, 033004 (2015).

[3] R.C. Isler, G.R. McKee, N.H. Brooks, W.P. West, M.E. Fenstermacher, and R.D. Wood, Phys. Plasmas **4**, 2989 (1997).

[4] J.L. Terry, B. Lipschultz, A.Yu. Pigarov, S.I. Krasheninnikov, B. LaBombard, D. Lumma, H. Ohkawa, D. Pappas, and M. Umansky, Phys. Plasmas **5**, 1759 (1998).

[5] G.M. McCracken, M.F. Stamp, R.D. Monk, A.G. Meigs, J. Lingertat, R. Prentice, A. Starling, R.J. Smith, and A. Tabasso, Nucl. Fusion **38**, 619 (1998).

[6] D. Nishijima, U. Wenzel, M. Motoyama, N. Ohno, S. Takamura, and S.I. Krasheninnikov, J. Nucl. Mater. **290**–**293**, 688 (2001).

[7] N. Ohno, N. Ezumi, D. Nishijima, and S. Takamura, J. Phys. **48**, 127 (1998).

[8] J.F. Drake, Phys. Fluids **30**, 2429 (1987).

[9] A. Huber, K. McCormick, P. Andrew, M.R. de Baar, P. Beaumont, S. Dalley, J. Fink, J.C. Fuchs, K. Fullard, W. Fundamenski, L.C. Ingesson, G. Kirnev, P. Lomas, F. Mast, S. Jachmich, G.F. Matthews, Ph. Mertens, A. Meigs, V. Philipps, J. Rapp, G. Saibene, S. Sanders, R. Sartori, M.F. Stamp, W. Zeidner, and JET-EFDA Contributors, J. Nucl. Mater. **363-365**, 365 (2007).

[10] A. Huber, S. Brezinsek, M. Groth, P.C. de Vries, V. Riccardo, G. van Rooij, G.

Sergienko, G. Arnoux, A. Boboc, P. Bilkova, G. Calabro, M. Clever, J.W. Coenen, M.N.A. Beurskens, T. Eich, S. Jachmich, M. Lehnen, E. Lerche, S. Marsen, G.F. Matthews, K. McCormick, A.G. Meigs, Ph. Mertens, V. Philipps, J. Rapp, U. Samm, M. Stamp, M. Wischmeier, S. Wiesen, and JET-EFDA contributors, J. Nucl. Mater. **438**, S139 (2013).

[11] S.I. Krasheninnikov, M. Rensink, T.D. Rognlien, A.S. Kukushkin, J.A. Goetz, B. LaBombard, B. Lipschultz, J.L. Terry, and M. Umansky, J. Nucl. Mater. **266-269**, 251 (1999).

[12] M. Kotschenreuther, P.M. Valanju, S.M. Mahajan, and J.C. Wiley, Phys. Plasmas **14**, 072502 (2007).

[13] I. Katramados, G. Fishpool, M. Fursdon, G. Whitfield, V. Thompson, and H. Meyer, Fusion Eng. Des. **86**, 1595 (2011).

[14] V.A. Soukhanovskii, S.L. Allen, M.E. Fenstermacher, D.N. Hill, C.J. Lasnier, M.A. Makowski, A.G. McLean, W.H. Meyer, E. Kolemen, R.J. Groebner, A.W. Hyatt, A.W. Leonard, T.H. Osborne, and T.W. Petrie, J. Nucl. Mater. **463**, 1191 (2015).

[15] E. Havlíčková, W. Fundamenski, M. Wischmeier, G. Fishpool, and D. Coster, J. Nucl. Mater. **438**, S545 (2013).

[16] M. Kotschenreuther, P. Valanju, B. Covele, and S. Mahajan, Phys. Plasmas **20**, 102507 (2013).

[17] Y. Hayashi, H. Nishikata, N. Ohno, and S. Kajita, Plasma Fusion Res. **11**, 1202005 (2016).

[18] N. Ohno, D. Nishijima, S. Takamura, Y. Uesugi, M. Motoyama, N. Hattori, H. Arakawa, N. Ezumi, S. Krasheninnikov, A. Pigarov, and U. Wenzel, Nucl. Fusion **41**, 1055 (2001).

[19] N. Ezumi, N. Ohno, K. Aoki, D. Nishijima, and S. Takamura, Contrib. Plasma Phys. **38**,

31 (1998).

[20] N. Ohno, N. Tanaka, N. Ezumi, D. Nishijima, and S. Takamura, Contrib. Plasma Phys. **41**, 473 (2001).

[21] A. Okamoto, S. Kado, Y. Iida, and S. Tanaka, Contrib. Plasma Phys. **46**, 416 (2006).

[22] H. Nishikata, 2017. Master thesis (in Japanese), Nagoya University, Nagoya, Japan.

[23] K-S. Chung, and I.H. Hutchinson, Phys. Rev. A **38**, 4721 (1988).

[24] K-S. Chung, and I.H. Hutchinson, Phys. Fluids B **3**, 3053 (1991).

[25] I.H. Hutchinson, Plasma Phys. Control. Fusion **44**, 1953 (2002).

[26] E.-K. Park, H.-J. Woo, K.-S. Chung, H. Tanaka, S. Kajita, and N. Ohno, Curr. Appl. Phys. **12**, 1497 (2012).

[27] D. Nishijima, U. Wenzel, K. Ohsumi, N. Ohno, Y. Uesugi, and S. Takamura, Plasma Phys. Control. Fusion **44**, 597 (2002).

[28] N. Asakura, S. Sakurai, N. Hosogane, M. Shimada, K. Itami, Y. Koide, O. Naito, Nucl. Fusion **39**, 1983 (1999).

[29] H. Meyer, I.G. Abel, R.J. Akers, A. Allan, S.Y. Allan, L.C. Appel, O. Asunta, M. Barnes, N.C. Barratt, N. Ben Ayed, J.W. Bradley, J. Canik, P. Cahyna, M. Cecconello, C.D. Challis, I.T. Chapman, D. Ciric, G. Colyer, N.J. Conway, M. Cox, B.J. Crowley, S.C. Cowley, G. Cunningham, A. Danilov, A. Darke, M.F.M. De Bock, G. De Temmerman, R.O. Dendy, P. Denner, D. Dickinson, A.Y. Dnestrovsky, Y. Dnestrovsky, M.D. Driscoll, B. Dudson, D. Dunai, M. Dunstan, P. Dura, S. Elmore, A.R. Field, G. Fishpool, S. Freethy, W. Fundamenski, L. Garzotti, Y.C. Ghim, K.J. Gibson, M.P. Gryaznevich, J. Harrison, E. Havlíčková, N.C. Hawkes, W.W. Heidbrink, T.C. Hender, E. Highcock, D. Higgins, P. Hill, B. Hnat, M.J. Hole, J. Horáček, D.F. Howell, K. Imada, O. Jones, E.

Kaveeva, D. Keeling, A. Kirk, M. Kočan, R.J. Lake, M. Lehnen, H.J. Leggate, Y. Liang, M.K. Lilley, S.W. Lisgo, Y.Q. Liu, B. Lloyd, G.P. Maddison, J. Mailloux, R. Martin, G.J. McArdle, K.G. McClements, B. McMillan, C. Michael, F. Militello, P. Molchanov, S. Mordijck, T. Morgan, A.W. Morris, D.G. Muir, E. Nardon, V. Naulin, G. Naylor, A.H. Nielsen, M.R. O'Brien, T. O'Gorman, S. Pamela, F.I. Parra, A. Patel, S.D. Pinches, M.N. Price, C.M. Roach, J.R. Robinson, M. Romanelli, V. Rozhansky, S. Saarelma, S. Sangaroon, A. Saveliev, R. Scannell, J. Seidl, S.E. Sharapov, A.A. Schekochihin, V. Shevchenko, S. Shibaev, D. Stork, J. Storrs, A. Sykes, G.J. Tallents, P. Tamain, D. Taylor, D. Temple, N. Thomas-Davies, A. Thornton, M.R. Turnyanskiy, M. Valovič, R.G.L. Vann, E. Verwichte, P. Voskoboynikov, G. Voss, S.E.V. Warder, H.R. Wilson, I. Wodniak, S. Zoletnik, R. Zagôrski, and the MAST and NBI Teams, Nucl. Fusion **53**, 104008 (2013).

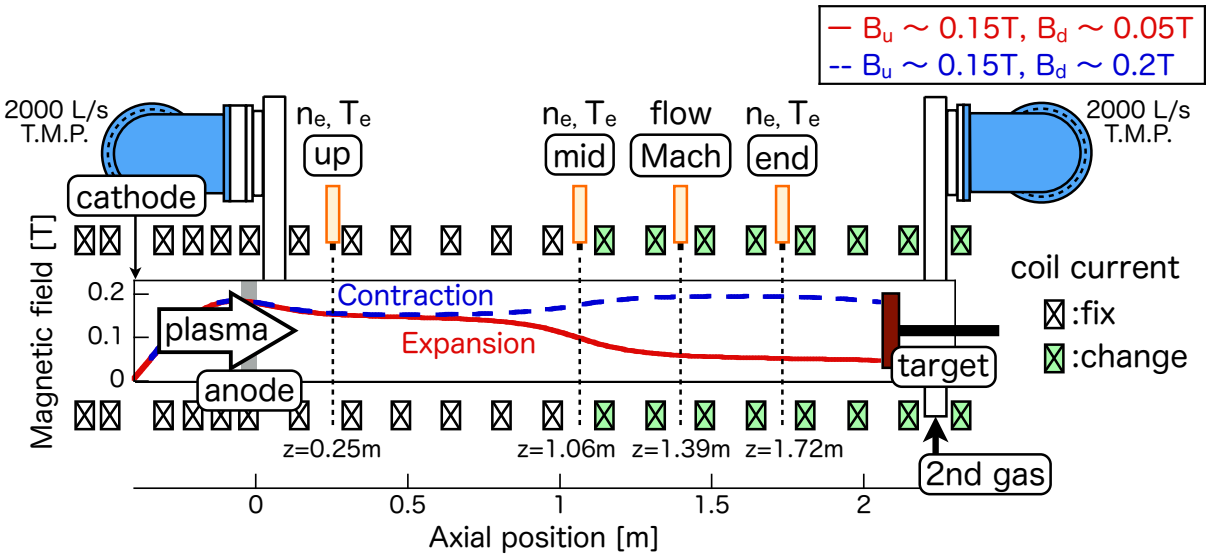

FIG. 1: (color online) Schematics view of the linear plasma device NAGDIS-II and the axial profiles of magnetic field strength at the center of the vacuum vessel when the magnetic flux is expanding (solid line) and contracting (dashed line). (Double column)

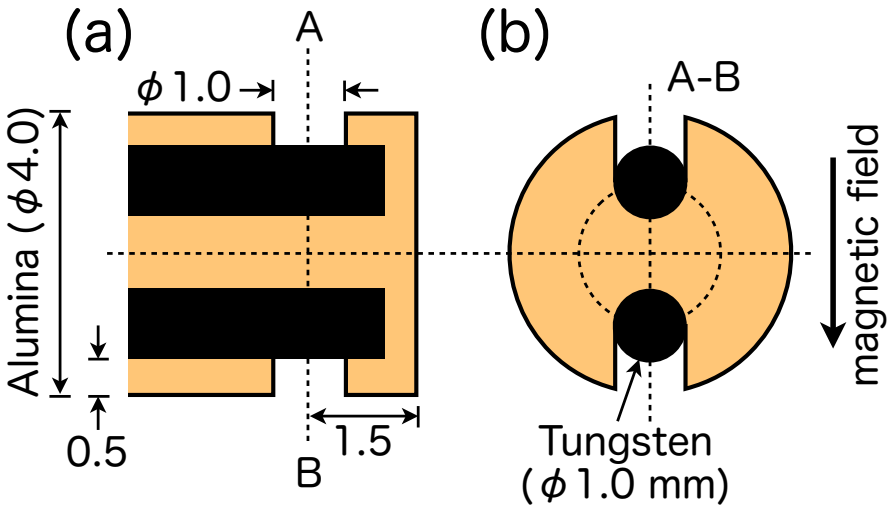

FIG. 2: (color online) Schematic view of the Mach probe head designed for measurements of axial flow velocity. (a) Side view and (b) cross section in the A and B planes as seen in (a). (Single column)

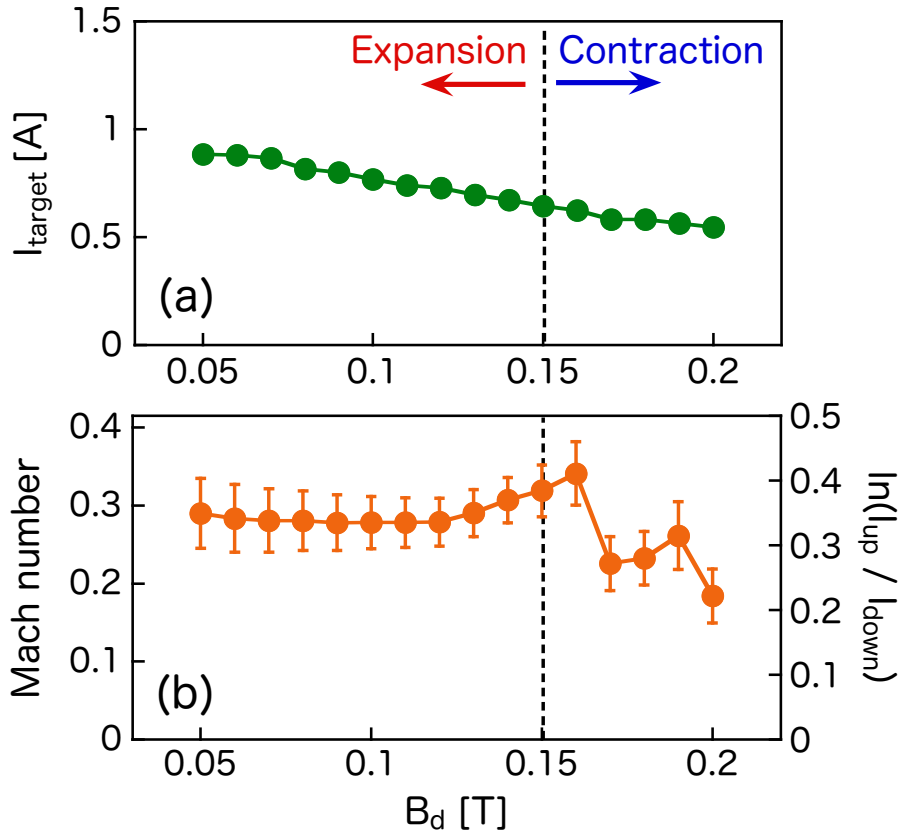

FIG. 3: (color online) (a) B_d dependence of current to the target plate (I_{target}) where the applied bias voltage was –100 V and (b) the flow velocity at z = 1.39 m by using the Mach probe. Mach numbers were evaluated by averaging Mach numbers calculated by intervals of 10 μs over the acquisition time of 1s. An error bar in a Mach number represents the standard deviation. The interval of 10 μs was determined so that steady flows could be assumed under the attached plasma condition. (Single column)

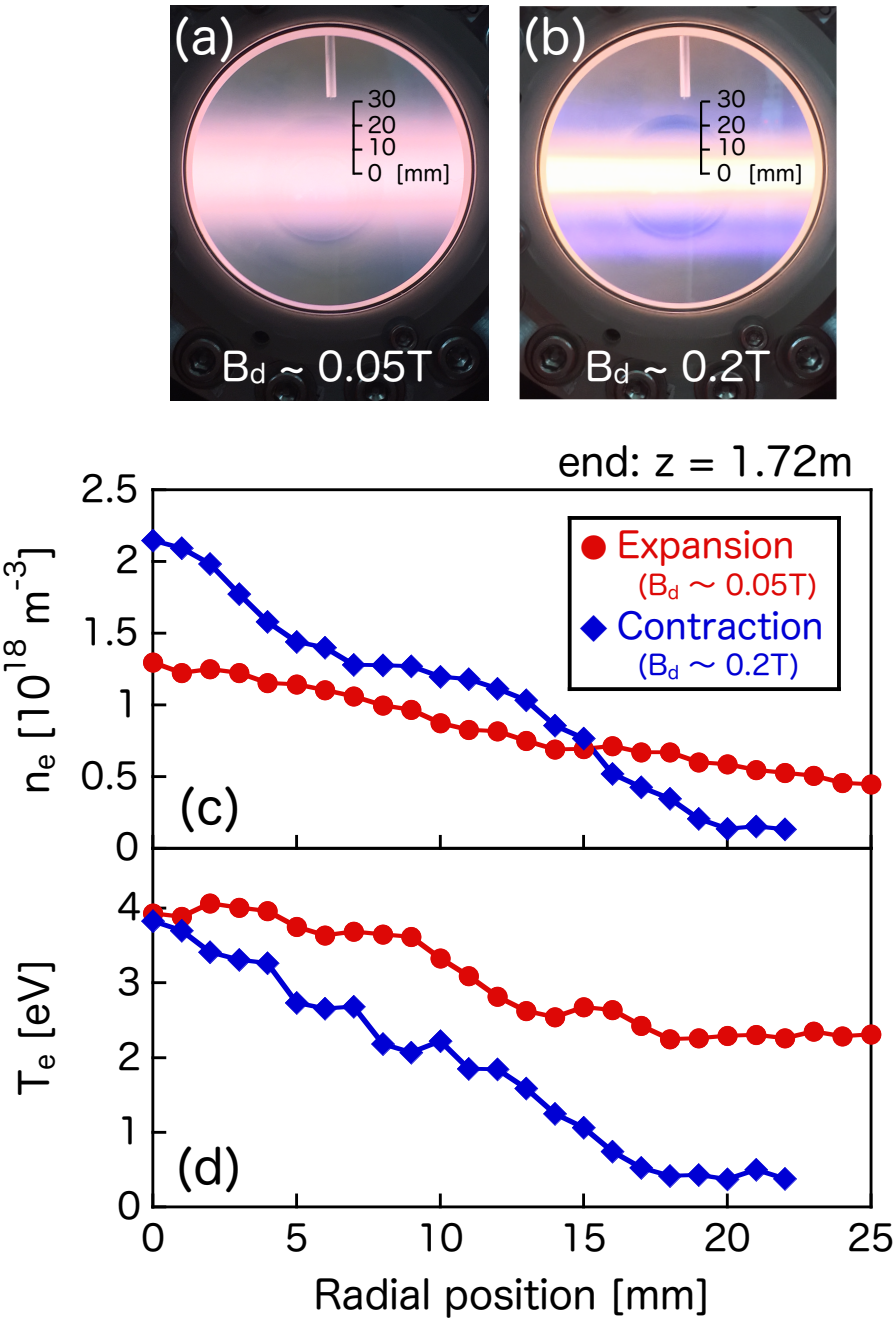

FIG. 4: (color online) Plasma pictures taken at $z \sim 1.39$ m when B_d (a) ~ 0.05 T and (b) ~ 0.2 T, the radial profiles of (c) n_e and (d) T_e at $z = 1.72$ m measured by using the double probe. (Single column)

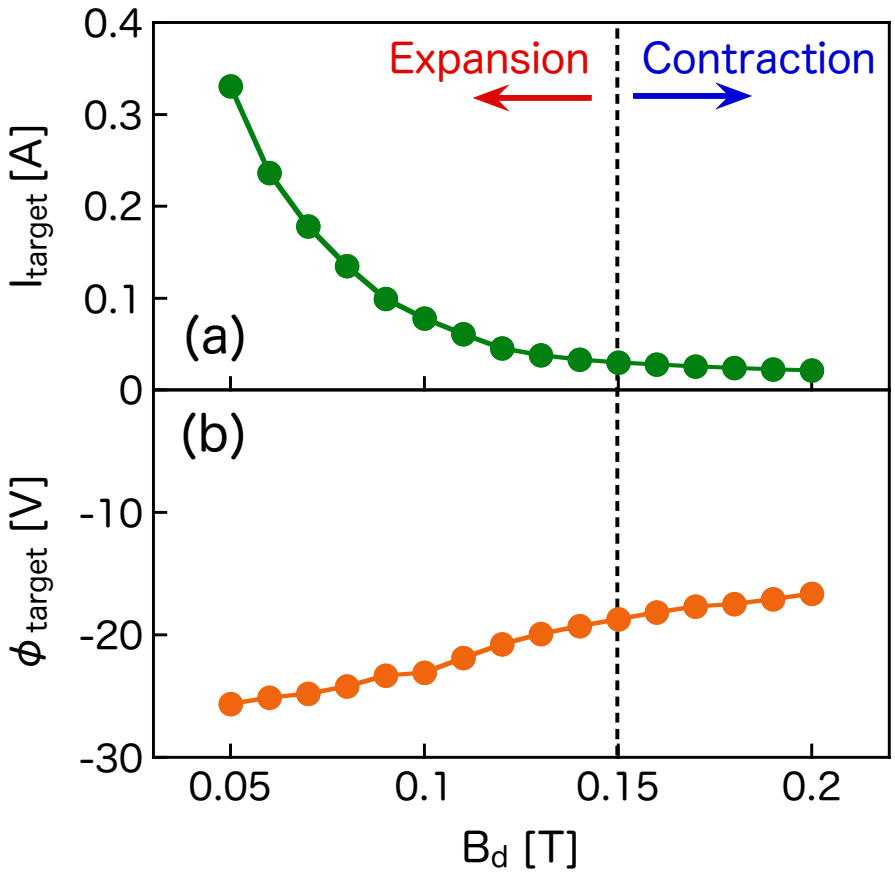

FIG. 5: (color online) (a) Current to the target plate (I_{target}) with an applied bias voltage of –200 V and (b) floating potential at the target plate (ϕ_{target}) as a function of B_d. (Single column)

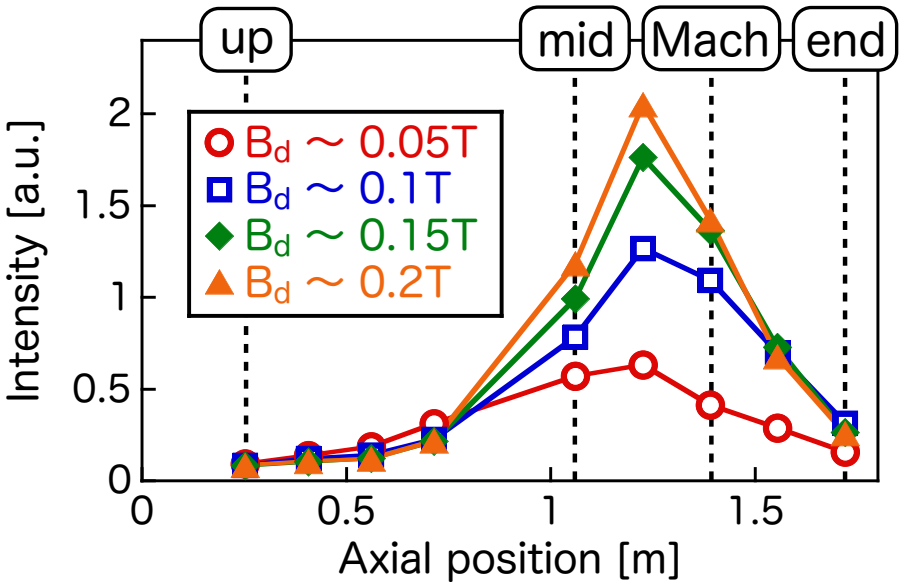

FIG. 6: (color online) Axial profiles of He-I line emission intensity corresponding to the transition from a highly excited level (370.5 nm: 2^3P-7^3D), while B_d was changed from 0.05 T to 0.2 T. The measurement positions for fast scanning electrostatic probes are shown. (Single column)

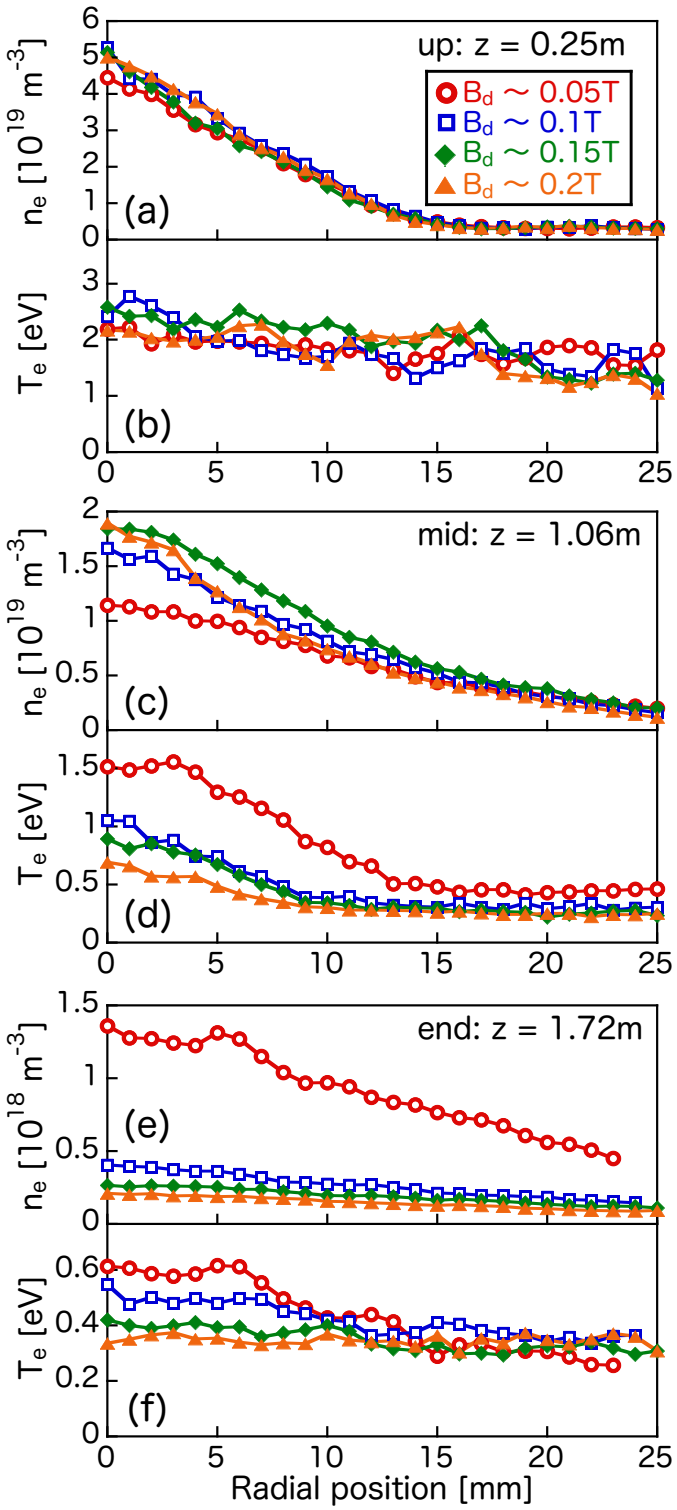

FIG. 7: (color online) Radial profiles of (a) n_e and (b) T_e at z = 0.25 m, (c) n_e and (d) T_e at z = 1.06 m, and (e) n_e and (f) T_e at z = 1.72 m, when B_d was changed from 0.05 T to 0.2 T. (Single column)

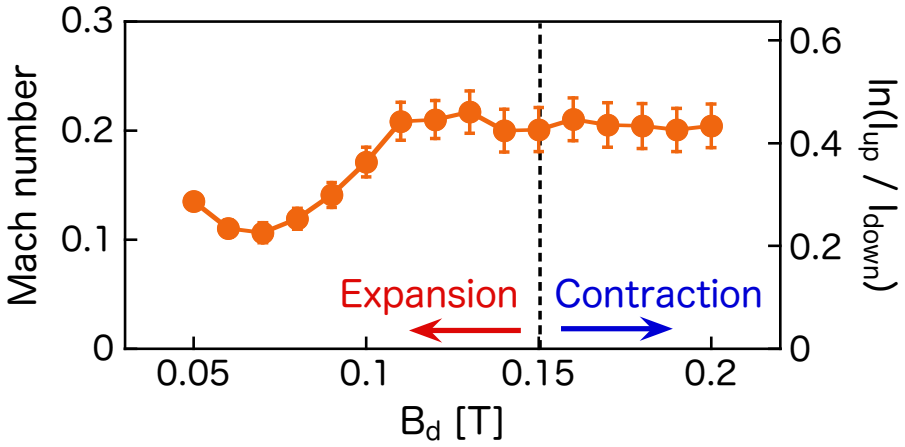

FIG. 8: (color online) Flow velocity measured at z = 1.39 m as a function of B_d. Mach numbers were evaluated by averaging Mach numbers calculated by intervals of 1 ms over the acquisition time of 1s. An error bar represents the standard deviation. The longer interval of 1 ms than that in attached plasma case was due to fluctuation which degraded the accuracy of I_{up}/I_{down} under the detached plasma condition. (Single column)

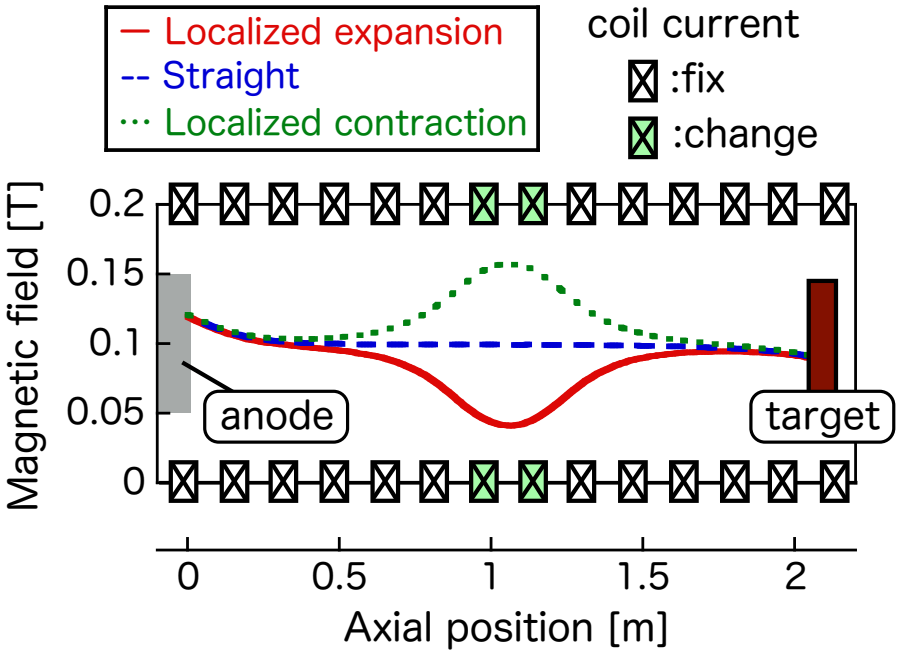

FIG. 9: (color online) Axial profiles of magnetic field strength at the center of vacuum vessel for producing the axially localized contracting and expanding magnetic fields in the NAGDIS-II device. (Single column)